Geoscientific
Model Development
Open Access
Discussions

Air quality forecasts at kilometer scale grid over Spanish complex terrains

M. T. Pay[1,*], F. Martínez[1], M. Guevara[1], and J. M. Baldasano[1,2]

[1]Earth Sciences Department, Barcelona Supercomputing Center-Centro Nacional de Supercomputación, Barcelona, Spain
[2]Environmental Modeling Laboratory, Technical University of Catalonia, Barcelona, Spain
[*]now at: Laboratoire de Météorologie Dynamique, École Polytechnique, Palaiseau Cedex, France

Correspondence to: M. T. Pay (maria.pay@bsc.es)

Title Page

Abstract	Introduction
Conclusions	References
Tables	Figures

◀ | ▶

◀ | ▶

Back | Close

Full Screen / Esc

Printer-friendly Version

Interactive Discussion

Abstract

CALIOPE-AQFS represents the current state-of-the-art in air quality forecasting systems running at high resolution over high performance computing platforms. It provides 48 h forecast of main pollutants over Spain at 4 km horizontal resolution, and over the most populated areas with complex terrains in Spain (Barcelona, Madrid and Andalucia domains) at 1 km. Increased horizontal resolution from 4 km to 1 km over the aforementioned domains leads to finer texture and more realistic concentration maps, justified by the increase of NO_2/O_3 spatial correlation coefficients from 0.79/0.69 (4 km) to 0.81/0.73 (1 km). High resolution emissions using the bottom-up HERMESv2.0 model are essential to improve the model performance when increasing resolution at urban scale, but it is not sufficient. Decreasing grid spacing does not reveal the expected improvement on hourly statistics, decreasing NO_2 bias only in $\sim 2\,\mu g\,m^{-3}$ and increasing O_3 bias in $\sim 1\,\mu g\,m^{-3}$. The grid effect is less pronounced for PM_{10} because part of its mass consists of secondary aerosols which are less affected by a decreasing grid size in contrast to the locally emitted primary components. The resolution increase has the highest impact over Barcelona, where air flow is mainly controlled by mesoscale phenomena and a lower PBL. Despite the merits and potential uses of the 1 km simulation, the limitations of current model formulations do not allow confirming their expected superiority close to highly urbanized areas and large sources. Future work should combine high grid resolution with techniques that decrease subgrid variability and models that consider urban morphology and thermal parameters.

1 Introduction

Recently World Health Organization (WHO) has shown that there are sufficient evidences supporting that particulate matter (PM), ozone (O_3) and nitrogen dioxide (NO_2) affect human health (WHO, 2013). Although NO_2 and PM concentrations improved from 2002 to 2011 in Europe, the situation is still far from matching the WHO air quality

Full Screen / Esc

Printer-friendly Version

Interactive Discussion

guidelines (AQG). The European annual limit values for NO_2 (annual) and PM_{10} (daily) were exceeded at 42–43 % of traffic stations in 2011. For the same year, about 33 % of the European urban population was exposed to PM_{10} concentration above the daily limit value and near 88 % was exposed to the respective WHO AQG (EEA, 2013).

5 Air pollution legislation for the protection of the increasing city population has recently increased the demand for urban air pollution forecasting systems to assess and understand its dynamics, alert the population when health-related issues occur, and developing emission abatement plans (EEA, 2011).

When applying an air quality modeling system, the definition of the grid resolution is

10 an important decision, the potential benefits of higher-resolution modeling should be weighed against the increased complexity on the inputs, CPU time, and disk space requirements. In theory, higher resolution modeling is expected to yield better forecasts because of better resolved model input fields (topography, land cover and emissions), and better mathematical characterization of physical and chemical processes. Further-

15 more, high resolutions (ranging from 1 to 5 km) are essential to reproduce mesoscale phenomena, e.g. those controlling O_3 transport along the mountainous northeastern Mediterranean coast (Fay and Neunhäuserer, 2006; Jiménez et al., 2006). Even with the finest scale, the modeled concentrations are not necessary the best (Mass et al., 2002; Gego et al., 2005; Valari and Menut, 2008) because by increasing emission and

20 meteorology spatial resolution, uncertainties can also increase with the risk of model performance.

Several studies have evaluated the impact of increasing horizontal resolution on different scales over eastern and southeastern USA using CMAQ and CAMx ranging from 32–12–4 km (Cohan et al., 2006; Tesche et al., 2006; Queen and Zhang, 2008). They

25 found no significant changes for O_3 and PM (< 5 % on average) and those changes were even lower between 12 km and 4 km (< 3 %). Concerning PM components, Fountoukis et al. (2013) found that increasing resolution provides differences mostly for primary PM rather than secondary PM. Recently, a model intercomparison exercise, named ScaleDep, has been performed to determine the effect of grid resolution in

Discussion Paper | Discussion Paper | Discussion Paper | Discussion Paper |

[GMDD](#)

7, 2293–2334, 2014

Air quality forecasts

M. T. Pay et al.

Title Page

Abstract   Introduction

Conclusions   References

Tables   Figures

◄   ►

◄   ►

Back   Close

Full Screen / Esc

Printer-friendly Version

Interactive Discussion

air quality modeling performance over Europe at regional and urban scale (Cuvelier et al., 2013). The exercise, involving five Chemical Transport Models (CTMs) (EMEP, CHIMERE, CMAQ, LOTOS-EUROS and RCGC) running under the same conditions over the full year 2009 at four resolutions (56, 28, 14, and 7 km), showed that it is difficult to define a grid size that is adequate to resolve the urban signal under all conditions affecting Europe, but 14 km resolution seems to be a good compromise between background applications and those reproducing most of the urban signals (7 km resolution). However, the ScaleDep exercise did not distinguish between different topographies or complex meteorological patterns, as characterized the Iberian Peninsula.

Few studies have been performed over selected areas in Spain, and they are mainly focused on O_3 and NO_2. Vivanco et al. (2008) evaluated the annual impact of increasing the resolution (at 36, 19, and 7 km) over Madrid on NO_2 and O_3 using the WRF-CHIMERE model by means of the disaggregation of EMEP emission inventory considering land use information. They showed that the model improvement is higher for NO_2 than O_3, and the most significant improvement is achieved when resolution increases from 36 to 19 km rather than to 7 km, linked to the increase of uncertainty in emission data introduced with the disaggregation techniques. Jiménez et al. (2006) used the MM5-CMAQ model to assess the influence of grid resolution on O_3 (at 8, 4, and 2 km) over the complex terrain of northeastern Iberian Peninsula (Catalonia) by means of a bottom-up emission model (EMICAT2000) during a summer pollution episode. They indicate that 2 km resolution improves the capability of the model to simulate exceedances of European limit values due to a better performance of the mesoscale phenomena and a better allocation of emissions. An important issue in both studies is the emission modeling approach (top-down vs. bottom-up) when applying high resolution at local scale (< 10 km). As Fountoukis et al. (2013) and Timmermans et al. (2013) demonstrate, in the range of local scale (e.g. Paris Greater area) the grid resolution is not currently the major source of discrepancies in model performance, but bottom-up emission inventories provide better performance and larger spatial concentration than down-scaled inventories. If local variation in input data (e.g. emission patterns or land

Air quality forecasts

M. T. Pay et al.

use) cannot be properly characterized, modeling with a finer grid resolution may not be greatly advantageous.

Increasing resolution is a technical challenge since the computational cost markedly increases with the inverse of the grid spacing. The current progress in computation allows increasing model resolution and investigating multiple spatial scales with the aim to establish the adequate grid size to forecast air quality at local scales. Recently, Colette et al. (2014) have evaluated the impact of increasing resolution till 2 km over the European continent using the CHIMERE model for an air pollution episode in 2009 using 2 million grid cells over 2000 CPUs of a high performance computing system hosted by the French Research and Technology Computing (CCRT/CEA).

The horizontal resolution is critical in terms of computational resources to an operational air quality forecast. In Europe, operational air quality systems use resolution between 12–25 km; meanwhile application to a single country can reach resolution between 4–10 km (Zhang et al., 2012). Over Spain, there are three systems providing air quality forecasts running at different horizontal resolutions. The lowest resolution system is OPANA, running at 27 km × 27 km at the Technical University of Madrid based on the MM5/CMAQ/EMIMO models (San José et al., 2009), followed by the Spanish meteorological office's system (AEMET, http://www.aemet.es/es/eltiempo/prediccion/calidad_del_aire) which provides forecast at 10 km × 10 km using the HIRLAM-HRN/MOCAGE/GEMS-TNO models. The CALIOPE Air Quality Forecast System (CALIOPE-AQFS; Baldasano et al., 2011; Pay et al., 2012a; and references therein) runs at the highest resolution, 4 km × 4 km, at the Barcelona Supercomputing Center-Centro Nacional de Supercomputación (BSC-CNS), and it bases on the WRFv3.5/CMAQv5.0.1/HERMESv2.0/BSC-DREAM8bv2 models. Moreover, CALIOPE-AQFS provides forecast at 1 km × 1 km resolution for Madrid and Barcelona metropolitan areas (since 2009), and Andalucia region (since 2013). Such resolution has been possible thanks to the high performance computing resources at the BSC-CNS and the availability of detail information of emission data over Spain.

The previous works demonstrate there is not a single answer which explains the merit of high-resolution modeling for all applications. The present work aims to assess the impact of increasing the horizontal resolution from 4 km to 1 km over areas affected by heterogeneous emission patterns and complex terrains such as Barcelona and Madrid metropolitan areas (BCN and MAD) together with the Andalucia region (AND). For that purpose, CALIOPE-AQFS forecasts pollutant concentrations (O_3, NO_2, and PM_{10}) at two horizontal resolutions, first at 4 km resolution covering Spain (IP4), and second at 1 km resolution involving AND, BCN, and MAD domains. The study is performed over April 2013, presenting seven days air pollution episode. We use observation from routine air quality monitoring networks to evaluate both resolutions.

Section 2 describes the configuration and computational setup of CALIOPE-AQFS; it analyses the domains and the period under study; and it defines the methodology used to evaluate the resolution increase. Section 3 quantifies the impact of resolution increase to forecast hourly concentrations (and exceedances) by pollutant, domain, building density and major emission sources. Section 4 concludes with the main results and some recommendations.

2 Methodology

2.1 Domain and period under study

Figure 1 shows the main NO_2 emission patterns and topographic characteristics of the domains at hands: Barcelona and Madrid metropolitan areas (BCN and MAD) and Andalucia region (AND). BCN is a coastal area characterized by several valleys perpendicular to the coastal line, with one coastal (500 m) and one pre-coastal (1000–1700 m) mountain range, which induce mesoscale phenomena such as sea-breeze and mountain-valley winds. On the other hand, MAD is a continental region with a much simpler topography (Central System located in the north-western area of the domain,

Air quality forecasts

M. T. Pay et al.

with summits reaching 2500 m and the Tajo valley in the southern area), which brings different locally-driven flows.

The urban contribution in BCN (3.1 million inhabitants) is accompanied by industrial and power generation emissions, the road network and the harbor; meanwhile MAD, the Spanish capital, is mainly under the influence of emission from the urban area (5.8 million inhabitants) and the road network that connects MAD with surrounding logistic and industrial activities and urban areas.

AND is the southern-most region in Spain with complex topography characterized by the large depression of the Guadalquivir Basin (delimited by the Iberian Massif and the Betic Range) that crosses the region from NE to SW along 60 km. About three quarters of AND has a mountainous orography, including Sierra Nevada (3481 m). AND includes one of the five biggest cities in Spain such as Seville ($\sim 700\,000$ inhabitants) and important industrial areas devoted to industrial processes, electric generation and maritime traffic such as Strait of Gibraltar.

The study is performed over April 2013. At the beginning and end of the month, the synoptic circulation was controlled by a low pressure system displaced over the south of British Isles that affect Western Europe leading to atmospheric instability over the IP. This pattern is typical of transitional months such as April and November (García-Valero et al., 2012; Valverde et al., 2014), which produces precipitation and decreases temperature because of the entrance of cold and humid wind from the Atlantic Ocean. In contrast, from 12–18 April there was a high pressure system crossing the Iberian Peninsula in a SW–NE direction, transporting dust from the Saharan desert and increasing temperature up to 25–28 °C. During the latter episode, available air quality stations at the study domains displayed several exceedances of the European limit values (8 exceedances of the NO_2 hourly limit value, 25 exceedances of the O_3 information threshold, and 31 exceedances of the PM_{10} daily limit value).

2.2 CALIOPE-AQFS

CALIOPE-AQFS provides 48 h air quality forecasts for Europe and Spain since October 2006 (www.bsc.es/caliope). It has been described and evaluated in detail elsewhere (Baldasano et al., 2008, 2011; Pay et al., 2011, 2012a). Briefly, it integrates a meteorological model (WRF-ARW v3.5; Skamarock and Klemp, 2008), an emission model (HERMESv2; Guevara et al., 2013), a chemical transport model (CMAQv5.0.1; Byun and Schere, 2006; Appel et al., 2013), and a mineral dust atmospheric model (BSC-DREAM8bv2; Pérez et al., 2006; Basart et al., 2012) together in an air quality forecast system.

Figure 1 shows the working domains of CALIOPE-AQFS. First, CALIOPE-AQFS is run over Europe at 12 km × 12 km horizontal resolution using initial/boundary conditions from the Final Analyses of the National Centers of Environmental Prediction (FNL/NCEP) at 12:00 UTC provided at intervals of 6 h ($0.5° × 0.5°$) for meteorology, and from the global model LMDz-INCA2 ($3.75° × 2.5°$, Szopa et al., 2009) for chemistry. Then, CALIOPE-AQFS run at higher horizontal resolution over the Iberian Peninsula at 4 km × 4 km (IP4) using a one-way nesting. In the present work CALIOPE-AQFS runs at 1 km × 1 km over the domains at hands (AND, BCN and MAD) throughout a nesting over IP4. HERMESv2.0 forecasts anthropogenic emissions following a bottom-up methodology (point, linear and area) based on the year 2009, and biogenic emissions using MEGANv2.0.4 model (Guenther et al., 2006). Emissions are aggregated into 1 km grids for AND, BCN and MAD 1 km simulations, and into 4 km for IP4.

Vertically, WRF-ARW is configured with 38 sigma layers up to 50 hPa, with 11 characterizing the planetary boundary layer (PBL); meanwhile CMAQ vertical levels are obtained by collapsing from the 38 WRF levels to a total of 15 layers steadily increasing from the surface up to 50 hPa, with a first layer depth of 39 m.

The present WRF setup uses the Rapid Radiation Transfer Model (RRTM) and Dudhia for long- and short- wave, respectively; the Kain–Fritsch cumulus parameterization

Title Page

Abstract | Introduction

Conclusions | References

Tables | Figures

◄ | ►

◄ | ►

Back | Close

Full Screen / Esc

Printer-friendly Version

Interactive Discussion

(Kain and Fritsch, 1990), the single-moment 3-class (WSM3) microphysics scheme, the Noah land-surface model (NoahLSM) and the Yonsei University PBL scheme (YSU).

Currently, a new CMAQ version is being tested in the CMAS community, namely CMAQv5.0 (CMAQ, 2012). It includes substantial scientific improvements over the version 4.5, especially devoted to improving SOA formation and dynamic interactions of fine and coarse aerosol. Based on evaluation results with previous CMAQ versions (4.5 vs. 5.0) (Pay et al., 2012b), CMAQ has been updated to version 5.0.1 inside CALIOPE-AQFS, using the CB05 chemical mechanism (Yarwood et al., 2005), the AERO5 for aerosols modeling, as well as in-line photolysis calculation.

CALIOPE-AQFS considers desert dust contribution by means of the BSC-DREAM8bv2, which runs off-line at $0.5° \times 0.5°$ resolution covering Europe, North Africa and Middle East. Its outputs are mass conservative interpolated to the CMAQ's Lambert conformal conic grids to the required resolution and domain. After interpolating, the modeled PM_{10} concentration is the sum of Aitken, accumulation and coarse-mode modes from CMAQ and the corresponding BSC-DREAM8bv2 bins with a diameter $\leq 10 \mu m$ (Pay et al., 2012a).

2.3 Computational strategy

Running CALIOPE-AQFS at 4 and 1 km is a technical challenge. The simulations are run on MareNostrum supercomputer (Intel Xeon E5-2670, 16 CPUs and 64 GB RAM memory per node) at BSC-CNS. Table 1 depicts the computational requirements to forecast air quality at 48 h in the domains at hands. The numbers of CPUs are chosen to maximize CPU efficiency. Thanks to the parallelization of meteorological and air quality models, MareNostrum uses up to 256 CPUs. The most computational demanding domain is the AND at 1 km resolution (366×358 cells, 256 CPU max., and 300 min).

CALIOPE-AQFS runs after downloading the meteorological and chemical boundary conditions. It uses a soft reservation, so a different number of CPUs can be used thought the night without blocking them, usually capping at 512 CPUs. Due to its

variable nature and complex dependencies, the computational time to forecast 48 h for the 4 domains is usually about 8–9 h. For the April 2013 simulation, times add up to 2880 CPU h day^{-1}, or 86 400 CPU hours in one CPU (9.86 years). The storage used for the April 2013 output files was 6.13 TB ($\sim$ 200 GB day^{-1}).

2.4 Evaluation the resolution increase

The comparison between both CALIOPE-AQFS grid resolutions is done in terms of gas-phase and aerosol concentrations (O_3, NO_2, and PM_{10}). Modeled concentrations are compared against observations on an hourly basis. CALIOPE-AQFS operationally receives air quality measurements from Spanish administrative networks in near real time (NRT) without any quality data or quality control. For the present study, NRT measurements are filtered removing data before and after measurement interruptions or calibrations. Also, a cut-off threshold of 1 µg m^{-3} is applied to the observed concentrations to avoid unrealistic observations. After filtering, the number of stations is 48/30/36 for O_3, 51/42/42 for NO_2, and 52/15/33 for PM_{10} at AND/BCN/MAD.

The meteorological fields are evaluated for wind speed at 10 m (U10), wind direction (WD10) and temperature at 2 m (T2M) at 10 METAR stations located at airports (6/2/2 stations in AND/BCN/MAD). They are discussed in Sect. S1.

Figure 2 shows the location of the air quality and METAR stations over the domains at hands. The spatial representativeness of the air quality network is highly variable. The influence of the station type is based on two classifications of air quality monitoring stations, the environment type (rural, R; suburban, S; and urban; U), and the dominant emission source (traffic, T; industrial, I; and background, B) derived from the Council decision 97/100/EC Garber et al. (2002).

The evaluation is based on discrete statistics performed on an hourly basis. We consider the correlation coefficient (r), mean (absolute, relative, and fractional) biases (MB, MNBE, and MFB), and error (MAE, MNGE, and MFE). Root Mean Square Error (RMSE) is also calculated because it intensifies big differences between measured and observed concentrations.

In order to evaluate the effect of resolution increase on forecasted exceedances and non-exceedances of limit values established by the European legislation, we calculate categorical statistics based on comparisons with fixed concentration thresholds (T). The calculated statistics are the accuracy (A), the bias (B), the probability of detection (POD), the critical success index (CSI), and the false alarm ratio (FAR) whose formulas and descriptions are explained elsewhere in Kang et al. (2005) and Eder et al. (2006). The 2008/50/EC directive sets an information threshold of $180\,\mu g\,m^{-3}$ for maximum daily O_3 concentrations (Max 1 h O_3) and a target value of $120\,\mu g\,m^{-3}$ for the maximum daily 8 h running O_3 mean (Max 8 h O_3) which should not be exceeded on more than 25 days per year. It establishes a limit value of $200\,\mu g\,m^{-3}$ for maximum daily NO_2 concentrations (Max 1 h NO_2), and $50\,\mu g\,m^{-3}$ for the daily PM_{10} mean (Mean 24 h PM_{10}) that should not be exceeded more than 35 times per year. Therefore, categorical evaluation will be done for Max 1 h NO_2, Max 1 h and Max 8 h O_3, and Mean 24 h PM_{10}. Note that mean and maximum concentrations are calculated considering the 75 % of the values, i.e. at least 18 h values per day for Mean 24 h, Max 1 h, and Max 8 h; and 6 h for 8 h values as established the 2008/50/EC.

3 Concentration maps and spatial representativeness

To analyze the spatial differences between resolutions, Figs. 3, 4, and 5 show the monthly mean concentration maps for April 2013 over MAD, BCN and AND domains at 4 km (left panels) and 1 km (right panels) for NO_2, O_3, and PM_{10}, respectively.

The maps of NO_2 and PM_{10} at both resolutions display similar distribution along the MAD and BCN urban plumes. On-road traffic constitutes the main source of primary pollutants in MAD and BCN, HERMESv2.0 estimates that 75 % and 59 % of NO_x emissions are produced by on-road traffic in both domains, respectively. Consequently, the monthly mean O_3 concentration maps are conserved when the resolution increases, where the NO_x titration effect on O_3 is significant along highways and major point

sources. In AND, NO_2 and O_3 concentration along the shipping route crossing the Strait of Gibraltar towards the Mediterranean Sea are also conserved between resolutions.

However, the definition of NO_2 concentrations along highways connecting the biggest cities with the rest of the country and industrial sectors are better textured at 1 km simulation than at 4 km, especially along those roads from/to Barcelona (e.g. AP7 Mediterranean highway, C32 connecting the harbor and the airport) and Madrid (the A-2 and A-6 in the north, and the A-3, A-4 and A-5 in the south). In the same way, 1 km O_3 maps are significantly better textured than those at 4 km along highways because the titration effect is more significant at 1 km due to the less dilution within grid cells. The titration effect of NO_x on O_3 along the main sources is more forceful in BCN than in MAD given a BCN bigger concentration gradient as a result of complex topography and recirculation flows that accumulate pollutants.

The improvement of the definition along roads in AND is lower than that observed in MAD and BCN domains due to the fact that the AND domain is bigger and displays lower traffic emission sources than MAD or BCN domains. Regarding PM_{10}, the main component in AND is the dessert dust ($\sim 40\%$ in both resolutions) from North Africa because there were two episodes on 14–19 and 25–26 April affecting the IP, as shown by the S–N PM_{10} gradient (Fig. 5e and f). The desert dust is transported from long-range simulation with BSC-DREAM8bv2.

Over complex terrains, the 1 km simulation allows reproducing more realistic NO_2 concentration maps due to a more detailed topographic information input. For instance, the BCN 1 km simulation displays the lowest NO_2 concentration ($< 10\,\mu g\,m^{-3}$) along the coastal chain (500 m height) and pre-coastal chain (1000–1700 m), except for the city urban hill where concentration reach 20–40 $\mu g\,m^{-3}$. In contrast, 4 km simulation provides more smoothed NO_2 concentration without any concentration gradient. Thus, the 1 km simulation generates slightly higher O_3 background concentrations than 4 km along the BCN pre-coastal chain (66–70 vs. 70–74 $\mu g\,m^{-3}$), and across the Iberian Massif (AND) where O_3 map displays significant structure due to the higher resolution topography that shapes the basin and the on-road traffic along.

Figures 3, 4, and 5 include dots corresponding to mean concentrations at air quality stations that help to qualitatively evaluate the modeled spatial representativeness at both resolutions. Note the high accordance between NO_2 observations and the 1 km simulation near main suburban traffic roads (e.g. Vilafranca, Igualada, Manresa, Mataró at BCN). Regarding O_3, although observed concentrations depict an overall tendency of the model to underestimate concentration at both resolutions, the 1 km simulation displays higher accord with measurements at rural background stations (e.g. El Atazar, San Martín, Villa de Prado, Villarejo and Orosco stations in MAD), and at suburban traffic stations (e.g. Manresa, Igualada and Vilafranca in BCN, with modeled O_3 concentrations around 54–58 $\mu g\,m^{-3}$ at 1 km and 60–66 $\mu g\,m^{-3}$ at 4 km). For PM_{10}, comparisons with measurements depicts that modeled concentrations are underestimated over background areas, mainly out of the urban/suburban area, as already discussed in Pay et al. (2012). However, PM_{10} measurements at the urban/suburban stations of Vilafranca, Sant Celoni, and Mataró in BCN (14–16 $\mu g\,m^{-3}$) show a higher accordance at 1 km than at 4 km (12–14 $\mu g\,m^{-3}$ vs. 8–10 $\mu g\,m^{-3}$).

The monthly spatial variation of increasing resolution is quantitatively analyzed in Fig. 6 for NO_2, O_3 and PM_{10} over AND, BCN and MAD. Over all domains, the explained spatial variability improves as a function of resolution for NO_2 and O_3 sustained by the increase of the monthly r from 0.79 (4 km) to 0.81 (1 km) for NO_2, and from 0.69 to 0.73 for O_3. The slopes significantly improve with resolution increase from 0.72 (4 km) to 0.77 (1 km) for NO_2 and from 0.50 (4 km) to 0.54 (1 km) for O_3, dominated by the improvement of model behavior in urban stations, indicating that CALIOPE-AQFS explains better the magnitude of the variability between urban regions at 1 km. In contrast, for PM_{10} overall behavior, monthly r slightly decreases when resolution increase from 0.67 to 0.58. Although BCN and MAD improve spatial variability when resolution increases (r increase 0.01 and 0.4, respectively); the global correlation coefficient is mainly deviated by AND stations (52/100) where r decreases in 0.1 from 0.36 (4 km) to 0.26 (1 km). Despite the unfavorable effect of resolution increase in PM_{10} over AND, the NO_2 and O_3 show the highest absolute increase in spatial r in this domain from 0.62

(4 km) to 0.71 (1 km) for NO_2 and from 0.58 (4 km) to 0.64 (1 km) for O_3 (increasing r in 0.09 and 0.06, respectively).

4 Temporal evaluation

The present section discusses the temporal evaluation of the resolution increase by pollutant, environments, predominant emission sources, and study domain. Figure 7 summarizes the statistical evaluation.

4.1 Pollutant

Table 2 depicts the statistical evaluation by pollutant with a focus on the reproduction of high concentrations established by the European directive (2008/50/EC). Depending on the pollutant lifetime, as well as its variability and dependency on its precursors, increasing resolution shows different impacts. The resolution increase has a positive effect on NO_2 decreasing bias in $2.0\,\mu g\,m^{-3}$ (from -4.5 to $-2.5\,\mu g\,m^{-3}$), but increasing absolute (squared) errors in $0.3\,(0.9)\,\mu g\,m^{-3}$. This positive effect is sustained by the perceptual variability, where the MB (MFB) is reduced in 42 (19) %; whereas MAE (MFE) only increases in 2 (1) %. The correlation coefficient does not significantly change, which is obvious because emissions at both resolutions are modeled based on the same approach. The bias improvement at 1 km resolution is justified because the higher resolution leads to better emission allocation from point, linear or area sources; decreases the artificial dilution of emission compared to the larger grid area; and treats chemistry more properly near large emission sources due to the decrease of artificial dilution.

In contrast, the resolution increase has a negative effect on O_3 increasing biases and errors between 0.1–$0.8\,\mu g\,m^{-3}$ for hourly and Max 8 h O_3. Relative (fractional) biases and errors increase in 8 % (15 %) and 1 % (1 %), respectively, for hourly O_3; and 6 %

and 4 % for Max 1 h O_3. However, only the statistical evaluation is not enough to explain the impact of the resolution increase on O_3.

According to the categorical evaluation, only few exceedances of European target and limit values were detected for Max 1 h NO_2 (9), Max 1 h O_3 (25), and Mean 24 PM_{10} (31) in April 2013. Thus, categorical evaluation is performed on the temporal basis established in the European legislation, but using a T based on the 75p of the observed concentration in each case. T corresponds to 71 $\mu g\,m^{-3}$ for Max 1 h NO_2, 108 (101) $\mu g\,m^{-3}$ for Max 1 h (Max 8 h) O_3, and 27 $\mu g\,m^{-3}$ for Mean 24 h PM_{10}.

Overall, CALIOPE-AQFS underestimates exceedances at both resolutions, indicating that errors of missing observed exceedances are not totally resolved with resolution increase ($a < d$). The best performance is found for NO_2 Max 1 h, where bias (B) improves from 37 % (4 km) to 40 % (1 km).

For NO_2 Max 1 h, there are 953 observed exceedances ($b + d$) of the threshold ($T = 47\,\mu g\,m^{-3}$). Increasing the resolution increases the POD from 49 % (4 km) to 56 % (1 km). As POD, CSI studies the exceedances but in a more coherent way considering both false alarms and missing events. Both POD and CIS increase in a 14 and 20 % when increasing resolution. The opposite effect appears for O_3. Besides O_3 POD is relatively low, the POD decreases with resolution increase. From 1306 observed exceedances of the 108 $\mu g\,m^{-3}$ Max 1 h, CALIOPE-AQFS detects 112 exceedances at 4 km and only 96 at 1 km. Increasing resolution decreases POD and CIS by 22 and 25 % for O_3 Max 1 h; meanwhile they do not significantly change for O_3 Max 8 h and PM_{10} Mean 24 h.

FAR increases for NO_2 Max 1 h (from 40 % to 42 %) and a decrease for O_3 Max 1 h (from 27 % to 17 %) when resolution increases. In relative terms, this variability is more significant for O_3 Max 1 h (37 %) than for NO_2 Max 1 h (5 %), indicating that increasing resolution has a positive global effect in terms of failures by reducing these false exceedances.

The accuracy (A) remains almost constant when resolution increases due to different reasons. Regarding NO_2 and O_3, it is due to a stable sum of b and c, increasing the b

in detriment of c and vice versa. For NO_2, the number of hits (b) to forecast Max 1 h at 1 km is higher than 4 km (537 vs. 466), but the number of correct negatives at 1 km is lower than at 4 km (2439 vs. 2517). The resolution increase has the opposite effect on O_3 over b and c for both Max 1 h and Max 8 h.

4.2 PM_{10} components

The resolution increase has the lowest effect on PM_{10} hourly concentration and its exceedances (< 1 %). PM_{10} components are secondary inorganic aerosols (SIA) which include sulfate (SO4), nitrate (NO3) and ammonium (NH4); secondary organic aerosol (SOA), elemental carbon (EC), sea salt (SS), desert dust (DD), and primary PM (PPM). Figure 8a shows that resolution increase does not significant change the PM_{10} composition. DD remains as main the contributor (∼ 40–41 %), followed by PPM (22–24 %), SIA (∼ 21–22 %), SS (9–11 %), EC (∼ 4 %) and SOA (∼ 0.6 %). However, the resolution increase effect on PM_{10} component concentrations is different (Fig. 8b) depending on the origin, atmospheric cycle and the way they are modeled. DD concentrations do not change between resolutions because it is mass conservative interpolated from $0.5° \times 0.5°$ till $1 \text{ km} \times 1 \text{ km}$.

Regarding SIA, the increasing resolution increases NO3 and NH4 concentration in 4 and ∼ 2 %, respectively and decreases SO4 in ∼ 2 %. The NH_4 increase with resolution means there are more primary precursors (H_2SO_4 or HNO_3/NO_2) available to neutralized NH_3 (gas) as NH4 (aerosol). However, the variability between SO4 and NO3 is more difficult to explain due to the nonlinearity of photochemistry and aerosol formation, controlled in some extent by the ISORROPIA thermodynamic equilibrium. Furthermore, the absence of aerosol measurements for April does not allow us to explain this situation.

The resolution increase displays the highest decrease for SS (∼ 16 %). CMAQv5.0.1 simulates SS emission as a function of wind speed relative humidity (Gong, 2003; Zhang et al., 2005). Although no shown here, when resolution increase wind speed

Title Page

Abstract | Introduction

Conclusions | References

Tables | Figures

|◄ | ►|

◄ | ►

Back | Close

Full Screen / Esc

Printer-friendly Version

Interactive Discussion

increases at available PM_{10} stations in $\sim 1.4/0.4/0.2\,\mathrm{m\,s^{-1}}$ in AND/BCN/MAD, and also over the open ocean.

For primary PM components (EC and PPM) increasing resolution depicts the highest increase in concentration (10 and $\sim 12\,\%$, respectively). As for NO_2, the 1 km simulation
5 leads to a reduced effect of artificially dilution of emission in a grid cell, so concentration gradient are stronger than at 4 km simulation.

4.3 Domain

Due to differences in geographical location and emission pattern over the domains at hands, the resolution increase has different impacts (Fig. 7). BCN shows the highest
10 NO_2 bias decrease (73 %) when the resolution increase, without affecting the correlation ($< 7\,\%$). However, O_3 shows significant variability over BCN, increasing r (4 %) and MB (23 %), and in a lesser extent increasing MB over AND (8 %); meanwhile over MAD the variability is reduced ($< 4\,\%$). MB decreases for PM_{10} ($< 1\,\mathrm{\mu g\,m^{-3}}$) over the pure urban domains MAD (3 %) and BCN (16 %), and increases for AND (7 %).
15 Figure 9 analyzes the impact of resolution increase shows on daily cycles. Although PBL measurements are not available, PBL daily cycles are together displayed in order to find some correlations with pollutant daily variability. PBL reaches its maximum at midday, being higher in MAD (1600 m a.g.l.) followed by AND (1000 m a.g.l.) and BCN (900 m a.g.l.) due to the lamination of the PBL growth by the Mediterranean sea
20 breezes.

As shown in Sect. S1, air flow at BCN coastal domain is controlled by mesoscale phenomena like sea-breezes (day) and land-breezes (night) result of its complex topography and location which control the pollutant's transport (Baldasano et al., 1994; Millán et al., 1997; Gonçalves et al., 2009). NO_2 daily cycle displays high influence
25 of traffic emissions (Fig. 9). Both resolutions show the highest underestimations at morning peak (5–9 a.m.) ($\sim 20\,\mathrm{\mu g\,m^{-3}}$). Although the afternoon peak is well reproduced, there is an excessive variability at both resolutions, result of a problem with wind

direction. During the sea breeze period, the mean simulated wind was more easterly than westerly as registered by measurements (Sect. S1). Simulations by photochemical modeling systems are known not to reproduce faithfully the morning hours after sunrise and the evening hours after sunset when the mixing height experiences rapid changes. Increasing the resolution increases NO_2 concentration from $14\,\mu g\,m^{-3}$ (4 km) to $17\,\mu g\,m^{-3}$ (1 km) at morning hours after sunrise (5–9 a.m.) and at evening hours after sunset (5–9 p.m.). This behavior could be explained by the PBL variability when increasing the resolution which decreases PBL height in $\sim 33\,m$ for these hours.

NO_2 performance impacts on O_3 daily cycles in BCN, showing that 4 and 1 km simulations underestimate maximum O_3 concentration at midday (1–4 p.m.) in $\sim 20\,\mu g\,m^{-3}$, and overestimate minimum O_3 concentration at morning hours after sunrise (5–9 a.m.) in $\sim 20\,\mu g\,m^{-3}$. The resolution increase allows slightly decreasing O_3 concentration at night, maybe control by the PBL decreasing at 1 km during early morning and late afternoon where PBL is at minimum values. During these hours, titration effect of NO_2 on O_3 is more effective, improving O_3 overestimation at daily minimum which allows slightly increasing hourly r (2 %). However, O_3 underestimation increases at late afternoon, contributing to increase the hourly mean bias from $\sim 9\,\mu g\,m^{-3}$ (4 km) to $\sim 11\,\mu g\,m^{-3}$ (1 km).

BCN PM_{10} model underestimation is not systematic along the daily cycle (Fig. 9), showing a bias of $\sim 20/10\,\mu g\,m^{-3}$ at daytime/night time. The higher overestimation during daytime regard to night time cannot be explained with the current results, but it could be because of missing sources and problems with PBL overestimation and emission dilutions. The resolution increase allows reducing the bias in $\sim 1\,\mu g\,m^{-3}$ (16 %), especially during early morning and late afternoon, when the highest PBL variation is detected between resolutions. Although evaluation of T2M, U10 and WD10 indicates that resolution increase has a slightly negative effect over BCN (Sect. S1), results indicated that the reduction in artificial dilution of NO_2 emissions together with lower PBL high during the night and early morning at 1 km than at 4 km allows improving NO_2, O_3 and PM_{10} concentration decreasing their biases.

In AND the model at both resolutions underestimates observed NO_2 concentration along the daily cycle ($\sim 5\,\mu g\,m^{-3}$), with the highest underestimation at the morning peak ($\sim 25\,\mu g\,m^{-3}$) and the lowest at afternoon peak ($\sim 10\,\mu g\,m^{-3}$). The resolution increase reduces bias from -3.5 to $2\,\mu g\,m^{-3}$ (43%) and increases r in a 7% (from 0.39 to 0.41). As in BCN, NO_2 underestimation directly impacts on O_3 daily cycle that resolution increase cannot resolve, increasing the bias in $\sim 1\,\mu g\,m^{-3}$ dominated by morning hours. In the case of PM_{10}, the daily cycle indicates that bias is almost systematic along the daily cycle ($\sim 22\,\mu g\,m^{-3}$). The resolution increase increases bias less than 4% at late afternoon, maybe dominated by the PBL decrease. The improvement of temperature and wind speed (Sect. S1) together with a lower nocturnal and diurnal PBL high when the resolution increase allows improving NO_2, meanwhile O_3 and PM_{10} do not significantly change.

During April 2013, the MAD main flow was control by S-SW synoptic wind canalized by orographic barriers in the NW domain and the Tajo valley (Valverde et al., 2014). NO_2 daily cycle depicts high influence of traffic activity (Fig. 9), with significant model underestimation at both resolutions at morning/afternoon peaks ($\sim 15/10\,\mu g\,m^{-3}$). Note a good behavior of the model at afternoon peak in terms of mean and variability controlled by southeastern winds. NO_2 performance leads to a better O_3 daily cycles than in AND and BCN, especially at early morning, where the titration effect of NO_2 is more efficient due to the lower NO_2 morning peak underestimation compared to the other domains. Meanwhile modeled PM_{10} at both resolutions present a profile control by a traffic emission, observed concentration displays a more plane daily cycle, where model underestimation reaches $40\,\mu g\,m^{-3}$ in the morning. Increasing resolution shows a positive effect for NO_2 and PM_{10} increasing r in 0.01 and reducing MB and RMSE in 0.1–$0.2\,\mu g\,m^{-3}$. However, it depicts the lowest variability compared to the other domains ($< 5\%$ for bias, error and r), which is the result of a relatively simpler topography and meteorological transport.

4.4 Environment and major sources

Figure 7 shows that the resolution impact also depends on the type of area and the dominant emission source. Theoretically, meteorological fields for urban areas differ from those for surrounding rural areas because of different morphology (radiation trapping and wind profiles) and materials (heat storage) of their surfaces and different energy consumption (heat release).

Increasing resolution reduces NO_2 bias at suburban and urban stations in 1.8–2 $\mu g\,m^{-3}$ and in a lesser extent, at rural stations in 1.2 $\mu g\,m^{-3}$. The correlation coefficients also improve at suburban (from 0.48 to 0.52) and at rural stations (from 0.34 to 0.35). That is not surprising because the 1 km grid allows to better allocating land-use categories (urban vs. rural) and their fraction in a grid cell than 4 km grid. Relatively, NO_2 biases decreases at urban (background) stations in 39 % (65 %), but O_3 biases increase at 9 % (5 %), respectively. For PM_{10}, the resolution increase does not significantly change as a function of area type, depicting variation in biases and errors remaining $< \pm 4$ % ($< 0.5\,\mu g\,m^{-3}$).

Low improvement over urban stations is obvious because the NoahLSM land-surface model does not consider the effect of urban morphology or thermal parameters to accurate model meteorological fields. Modeling air quality at urban scale over cities requires a model that describes heat/momentum exchange between buildings and the lower atmospheric. For instance, the impact of using an urban model on meteorological fields over Paris Greater area was studied in Kim et al. (2013) using WRF with the Urban Canopy Model, demonstrating that overestimations of the wind speed were significantly reduced below 1000 m height.

The resolution increase effect is positive for the primary pollutant near important emission sources reducing NO_2 biases at traffic (industrial) stations in ~ 3 (2) $\mu g\,m^{-3}$, but increasing O_3 biases in ~ 2 (1) $\mu g\,m^{-3}$. However, the resolution increase in the range of 4–1 km has not the expected improvement in hourly statistical scores based on the constraints of the current model formulation that cannot resolve the subgrid air

quality variability just with increasing resolution. For instance, although on-road traffic emissions are estimated following a bottom-up approach along highways and routes, that heterogeneity is lost in the volume averaging process performed within CTM, which artificially dilutes emission rates over the grid cells. The resolution effect is the lowest

5 at background stations, which are not influenced by any single source, but rather by the integrated contribution from all sources upwind of the stations where variations are less than 1 % for O_3 and PM_{10} ($< 1\,\mu g\,m^{-3}$), but increasing background NO_2 levels in ($\sim 1\,\mu g\,m^{-3}$) from 4 km to 1 km (48 %).

Figure 10 shows temporal series and daily cycles for NO_2 and O_3 at traffic and

10 background stations over the episode 12–18 April 2013. At traffic stations, the temporal series show a remarkable O_3 daily cycle (observed $25p = 23.2\,\mu g\,m^{-3}$ and $75p = 77.5\,\mu g\,m^{-3}$) due to O_3 destruction leaded by high NO_x environments (observed $50p = 34.5\,\mu g\,m^{-3}$). In contrast, the NO_2-limited regime at background sites (observed $50p = 19\,\mu g\,m^{-3}$) allows higher O_3 concentrations (observed $25p = 38\,\mu g\,m^{-3}$

15 and $75p = 89\,\mu g\,m^{-3}$) than over high NO_2 environments.

During the episode, the resolution increase at traffic stations has a positive effect increasing correlation coefficient for NO_2 (from 0.73 to 0.76) and O_3 (from 0.83 to 0.86) and decreasing NO_2 mean bias in $\sim 5\,\mu g\,m^{-3}$ (from 6 to $1\,\mu g\,m^{-3}$). NO_2 daily cycle improves at morning hours after sunrise reducing bias in 5–$10\,\mu g\,m^{-3}$ and contributing to

20 reduce O_3 overestimation ($\sim 5\,\mu g\,m^{-3}$). In contrast, at background stations, where the NO_x/O_3 chemistry is less dominant, the resolution effect is not significant. Such behavior reflects that the horizontal resolution affects the representation of chemical processes near large emission sources, such as O_3 formation efficiency and nighttime O_3 titration, with an improved performance at finer resolution (Mathur et al., 2005). How-

25 ever, the loss of subgrid variability and improvement of meteorological fields (transport and temperature) are required.

Title Page

Abstract | Introduction

Conclusions | References

Tables | Figures

◀ | ▶

◀ | ▶

Back | Close

Full Screen / Esc

Printer-friendly Version

Interactive Discussion

5 Conclusions

The present work shows the effects of increasing the horizontal resolution from 4 km to 1 km using the CALIOPE-AQFS on pollutant concentrations (NO_2, O_3, and PM_{10}) over three Spanish domains (AND, BCN and MAD) in April 2013.

The global features of concentration maps at both resolutions are quite similar, with zones of high/low concentration identically located, which is obvious because both simulations are based on the same emission dataset. Further comparisons demonstrate the resolution increase provides better-defined and more realistic concentration structures over large sources (roads and industries) and complex terrains (defining sharper orographic hills). The titration effect on O_3 along highways and major point sources is better captured at the 1 km simulation than at 4 km, because the latter is affected by higher dilution within the grid cells. This improvement is quantified by the increase of spatial correlation coefficients in 3 (6) % for NO_2 (O_3).

However, the resolution increase in the range of 4–1 km has not the expected improvement in hourly statistical scores for any pollutant. Hourly correlation coefficients do not significantly change, and absolute (relative) errors and biases vary $< 2\,\mu g\,m^{-3}$ (9 %). The merit of the resolution increase may be underrated when classical statistics are applied at observation locations (Mass et al., 2002; Gego et al., 2005). For instance, although the structure of important NO_2 urban plumes ($> 40\,\mu g\,m^{-3}$) features often become more realistic (stronger and better defined plumes) as resolution increases, statistics are deeply degraded by even small timing and spatial error.

The resolution increase has a significant impact on reducing NO_2 hourly bias (in 42 %, $2\,\mu g\,m^{-3}$), without any significant change in error and r (< 2 %), but increases O_3 hourly biases ($< 1\,\mu g\,m^{-3}$). Main differences between resolutions appear at daytime and nighttime traffic peaks, when the mixing height experiences rapid changes, allowing the 1 km simulation to slightly reduce NO_2 underestimation in the morning by ~ 5–$10\,\mu g\,m^{-3}$. O_3 daily cycles at large sources depict a high influence of NO_2 hourly

concentration, increasing O_3 hourly bias in $\sim 3\,\mu g\,m^{-3}$. That behavior is controlled by the daytime O_3 underestimation and to lesser extent by the night time overestimation. Increasing the resolution allows reducing O_3 overestimations at night ($\sim 5\,\mu g\,m^{-3}$) partly due to higher nocturnal NO_2 concentrations.

5   Concerning the capability to forecast exceedances of 75p of the observed maximum 1 h concentration, the increased resolution has a positive effect, increasing the number of hits to forecast the exceedances of 75p of the observed NO_2 Max 1 h (537 vs. 466 over 953 exceedances) and reducing the false alarms for Max 1 h O_3 exceedances (FAR improves in 37 %).

10   The grid effect is less pronounced for PM_{10} than for NO_2 and O_3. The low increase ($< 0.1\,\mu g\,m^{-3}$) in monthly mean PM_{10} concentration when the resolution increases is the result of compensating biases of PM_{10} components, mainly controlled by the PPM and EC increase and the SS decrease.

    BCN is the domain where the resolution increase has the highest effect with bias (error) changes of 16–73 % (< 5 %), followed by AND with 4–43 % (< 5 %) and MAD < 3–5 % (< 1 %). In BCN, as in the western Mediterranean Basin, the distribution of O_3 and its precursors is governed by the mesoscale circulation. In that sense, the resolution increase has a great impact in BCN where induced mesoscale phenomena control the air flow; meanwhile synoptic transport is more important in MAD and AND. Benefits

20 of increasing the resolution till 1 km over rural areas (Mass et al., 2002) increases the realism of mesoscale meteorological structures like orographic wind and circulation. Over urban areas along the western Mediterranean coast (Toll and Baldasano, 2002; Jiménez et al., 2006; Fay and Neunhäuserer, 2006), the benefits of increasing resolution till 1 km require further improvements and urbanization steps.

25   In urban areas or near large emission sources (industrial and traffic stations), the NO_2 and O_3 concentrations are more sensitive to changes in grid resolution. The concentration increase in primary anthropogenic pollutants (NO_2, PPM and EC) is obvious since the high resolution allows a better allocation of emissions at point, linear and area sources, and decreases the artificial dilution of emission compared to the larger

grid area. However, the challenge of the 1 km simulation to more accurately describe the chemical formation of O_3 and dilution of NO_2 concentration in those areas was not generally successful.

This analysis demonstrates weakness in the current model formulations that cannot be resolved just with high-resolution modeling. The subgrid air quality variability at 1 km resolution is not reproduced along large emission sources or urban areas because finer spatial structure is expected but unresolved. There are some underlying problems. First, there is a loss of subgrid emission heterogeneity. Emission input to CTM is an average rate which accounts for the volume averaged quantity of mass released per unit of time. No other information regarding emission allocation (e.g. point, linear or per area) is considered; for instance a large amount of mass can be emitted by a small portion of the grid surface or by several sources scattered around it (Galmarini et al., 2008; Cassiani et al., 2010; Ching and Majeed, 2012). Despite the fact that emissions are estimated following a bottom-up approach emission model, the emission heterogeneity is lost in the volume averaging process performed within CTM, the loss is even higher when resolution decreases (from 1 km to 4 km). Second, there is a low degree of complexity in flow and dispersion details at urban scales, where most of the pollutants come from street canyons and/or tree canopies which are transported along until mixing conditions allow the pollutants to disperse above these urban canopy levels (Kim et al., 2013; Ching, 2013). Third, the US Geological Survey (USGS) land-use data is used by default in the WRF model is based on 1993, and the urban changes during the last 20 years over MAD and BCN are significant.

Since temperature and wind speed are very sensitive to the ratio of the building width to the road width, the next improvement should be focused on using an urban canopy model which considers the effect on the transfer of energy and momentum between the urban structures and the lower atmosphere, which is crucial for meteorology and air quality modeling. However, an urban canopy scheme and a canopy parameter database (urban fraction, building height and area) are necessary. In order to update the land-use data, the Coordination of Information on the Environment (CORINE) data

of European Environmental Agency should be used instead of the USGS following the methodology of Pineda et al. (2004).

Supplementary material related to this article is available online at http://www.geosci-model-dev-discuss.net/7/2293/2014/ gmdd-7-2293-2014-supplement.pdf.

References

Appel, K. W., Pouliot, G. A., Simon, H., Sarwar, G., Pye, H. O. T., Napelenok, S. L., Akhtar, F., and Roselle, S. J.: Evaluation of dust and trace metal estimates from the Community Multiscale Air Quality (CMAQ) model version 5.0, Geosci. Model Dev., 6, 883–899, doi:10.5194/gmd-6-883-2013, 2013.

Baldasano, J. M., Cremades, L., and Soriano, C.: Circulation of Air Pollutants over the Barcelona Geographical Area in Summer, in: Proceedings of Sixth European Symposium Physico-Chemical Behaviour of Atmospheric Pollutants, Varese (Italy), 18–22 October 1993, Report EUR 15609/1 EN, 474–479, 1994.

Baldasano, J. M., Jiménez-Guerrero, P., Jorba, O., Pérez, C., López, E., Güereca, P., Martín, F., Vivanco, M. G., Palomino, I., Querol, X., Pandolfi, M., Sanz, M. J., and Diéguez, J. J.: CALIOPE: an operational air quality forecasting system for the Iberian Peninsula, Balearic

Islands and Canary Islands – first annual evaluation and ongoing developments, Adv. Sci. Res., 2, 89–98, doi:10.5194/asr-2-89-2008, 2008.

Baldasano, J. M., Pay, M. T., Jorba, O., Gassó, S., and Jiménez-Guerrero, P.: An annual assessment of air quality with the CALIOPE modeling system over Spain, Sci. Total Environ., 409, 2163–2178, 2011.

Basart, S., Pérez, C., Nickovic, S., Cuevas, E., and Baldasano, J. M.: Development and evaluation of the BSC-DREAM8b dust regional modelo ver Northern Africa, the Mediterranean and the Middle East, Tellus B, 64, 1–12, 2012.

Byun, D. W. and Schere, K. L.: Review of the governing equations, computational algorithms and other components of the Models-3 Community Multiscale Air Quality (CMAQ) Modeling System, Appl. Mech. Rev., 59, 51–77, 2006.

Cassiani, M., Vinuesa, J. F., Galmarini, S., and Denby, B.: Stochastic fields method for sub-grid scale emission heterogeneity in mesoscale atmospheric dispersion models, Atmos. Chem. Phys., 10, 267–277, doi:10.5194/acp-10-267-2010, 2010.

Ching, J. K. S.: A perspective on urban canopy layer modeling for weather, climate and air quality applications, Urban Climate, 3, 13–39, 2013.

Ching, J. K. S. and Majeed, M. A.: An approach to characterized within-grid concentration variability in air quality models, Atmos. Environ., 49, 348–360, 2012.

CMAQ: Technical Documentation, available at: http://www.airqualitymodeling.org/cmaqwiki/index.php?title=CMAQ_version_5.0_(February_2012_release)_Technical_Documentation, last access 8 January 2014.

Cohan, D. S., Hu, Y., and Russel, A. G.: Dependence of ozone sensitivity analysis on grid resolution, Atmos. Environ., 40, 126–135, 2006.

Colette, A., Bessagnet, B., Meleux, F., Terrenoire, E., and Rouïl, L.: Frontiers in air quality modelling, Geosci. Model Dev., 7, 203–210, doi:10.5194/gmd-7-203-2014, 2014.

Cuvelier, C., Thunis, P., Karam, D., Schaap, M., Hendriks, C., Kranenburg, R., Fagerli, H., Nyíri, Á., Simpson, D., Wind, P., Schulz, M., Bessagnet, B., Colette, A., Terrenoire, E., Rouïl, L., Stern, R., Graff, A., Baldasano, J. M., and Pay, M. T.: ScaleDep: performance of European chemistry-transport models as function of horizontal spatial resolution, EMEP Report 1/2013, 63 pp., available at: http://emep.int/publ/reports/2013/MSCW_technical_1_2013.pdf, last access: 4 April 2013.

Eder, B., Kang, D., Mathur, R., Yu, S., and Schere, K.: An operational evaluation of the Eta-CMAQ air quality forecast model, Atmos. Environ., 40, 4894–4905, 2006.

Title Page

Abstract | Introduction

Conclusions | References

Tables | Figures

◀ | ▶

◀ | ▶

Back | Close

Full Screen / Esc

Printer-friendly Version

Interactive Discussion

EEA: The application of models under the European Union's Air Quality Directive: a technical reference guide, EEA Technical report 10/2011, Publication Office of the European Union, Luxembourg, ISSN Technical report series 1725–2237, ISBN 978-92-9213-223-1, doi:10.2800/80600, 76 pp., 2011.

EEA: Air quality in Europe – 2013 report, EEA Report 9/2013, ISSN 1725-9177, 112 pp., 2013.

Fay, B. and Neunhäuserer, L.: Evaluation of high-resolution forecasts with the non-hydrostaticnumerical weather prediction model Lokalmodell for urban air pollutionepisodes in Helsinki, Oslo and Valencia, Atmos. Chem. Phys., 6, 2107–2128, doi:10.5194/acp-6-2107-2006, 2006.

Fountoukis, C., Koraj, Dh., Denier van der Gon, H. A. C., Charalampidis, P. E., Pilinis, C., and Pandis, S. N.: Impact of grid resolution on the predicted fine PM by a regional 3-D chemical transport model, Atmos. Environ., 68, 24–32, 2013.

Galmarini, S., Vinuesa, J.-F., and Martilli, A.: Modeling the impact of sub-grid scale emission variability on upper-air concentration, Atmos. Chem. Phys., 8, 141–158, doi:10.5194/acp-8-141-2008, 2008.

Garber, W., Colosio, J., Grittner, S., Larssen, S., Rasse, D., Schneider, J., and Houssiau, M.: Guidance on the Annexes to Decision 97/101/EC on Exchange of Information as revised by Decision 2001/752/EC, Technical Report, European Commission, DG Environment, 2002.

García-Valero, J. A., Montávez, J. P., Jérez, S., Gómez-Navarro, J. J., Lorente-Plazas, R., and Jiménez-Guerrero, P.: A seasonal study of the atmospheric dynamics over the Iberian Peninsula based on circulation types, Theor. Appl. Climatol., 110, 219–310, 2012.

Gego, E., Hogrefe, C., Kallos, G., Voudouri, A., Irwin, J., and Rao, S. T.: Examination of model predictions at different horizontal grid resolutions, Environ. Fluid Mech., 5, 63–85, 2005.

Gonçalves, M., Jiménez-Guerrero, P., and Baldasano, J. M.: Contribution of atmospheric processes affecting the dynamics of air pollution in South-Western Europe during a typical summertime photochemical episode, Atmos. Chem. Phys., 9, 849–864, doi:10.5194/acp-9-849-2009, 2009.

Gong, S. L.: A parameterization of sea-salt aerosol source function for sub- and super-micron particles, J. Geophys. Res., 17, 197, 2003.

Guenther, A., Karl, T., Harley, P., Wiedinmyer, C., Palmer, P. I., and Geron, C.: Estimates of global terrestrial isoprene emissions using MEGAN (Model of Emissions of Gases and Aerosols from Nature), Atmos. Chem. Phys., 6, 3181–3210, doi:10.5194/acp-6-3181-2006, 2006.

Title Page

Abstract | Introduction

Conclusions | References

Tables | Figures

◄ | ►

◄ | ►

Back | Close

Full Screen / Esc

Printer-friendly Version

Interactive Discussion

Guevara, M., Martínez, F., Arévalo, G., Gassó, S., and Baldasano, J. M.: An improved system for modelling Spanish emissions: HERMESv2.0, Atmos. Environ., 81, 209–221, 2013.

Jiménez, P., Jorba, O., Parra, R., and Baldasano, J. M.: Evaluation of MM5-EMICAT2002-CMAQ performance and sensitivity in complex terrains: high-resolution application to the northeastern Iberian Peninsula, Atmos. Environ., 40, 5056–5072, 2006.

Kain, J. S. and Fritsch, J. M.: A one-dimensional entraining/detraining plume model and its application in convective parameterization, J. Atmos. Sci., 47, 2784–2802, 1990.

Kang, D., Eder, B. K., Stein, A. F., Grell, G. A., Peckham, S. E., and McHenry, J.: The new England air quality forecasting pilot program: development of an evaluation protocol and performance benchmark, J. Air Waste Mange. Assoc., 55, 1782–1796, 2005.

Kim, Y., Sartelet, K., Raut, J.-C., and Chazette, P.: Evaluation of the weather research and forecast/urban model over Greater Paris, Bound.-Lay. Meteorol., 149, 105–132, 2013.

Mathur, R., Shankar, U., Hanna, A. F., Odman, M. T., McHenry, J. N., Coats, C. J., Alapaty, K., Xiu, A., Arunachalam, S., Olerud Jr., D. T., Byun, D. W., Schere, K. L., Binkowski, F. S., Ching, J. K. S., Dennis, R. L., Pierce, T. E., Pleim, J. E., Roselle, S. J., and Young, J. O.: Multiscale Air Quality Simulation Platform (MAQSIP): initial applications and performance for tropospheric ozone and particulate matter, J. Geophys. Res., 110, D13308, doi:10.1029/2004JD004918, 2005.

Mass, C., Ovens, D., Albright, M., and Westrick, K.: Does increasing horizontal resolution produce better forecasts? the results of two years of real-time numerical weather prediction in the Pacific Northwest, B. Am. Meteorol. Soc., 83, 407–430, 2002.

Millán, M., Salvador, R., Mantilla, E., and Kallos, G.: Photooxidant dynamics in the Mediterranean basin in summer: results from European research projects, J. Geophys. Res., 102, 8811–8823, 1997.

Pay, M. T., Jiménez-Guerrero, P., and Baldasano, J. M.: Implementation of resuspension from paved roads for the improvement of CALIOPE air quality system in Spain, Atmos. Environ., 45, 802–807, 2011.

Pay, M. T., Jiménez-Guerrero, P., Jorba, O., Basart, S., Pandolfi, M., Querol, X., and Baldasano, J. M.: Spatio-temporal variability of levels and speciation of particulate matter across Spain in the CALIOPE modeling system, Atmos. Environ., 46, 376–396, 2012a.

Pay, M. T., Gassó, S., and Baldasano, J. M.: Evaluation of the CMAQ5.0 in the framework of the CALIOPE air quality forecasting system over Europe, in: 11th Annual CMAS Conference, Chapel Hill, North Carolina, USA, 15–17 October 2012, 2012b.

Air quality forecasts

M. T. Pay et al.

Title Page

Abstract | Introduction

Conclusions | References

Tables | Figures

◄◄ | ►►

◄ | ►

Back | Close

Full Screen / Esc

Printer-friendly Version

Interactive Discussion

Pérez, C., Nickovic, S., Baldasano, J. M., Sicard, M., Rocadenbosch, F., and Cachorro, V. E.: A long Saharan dust event over the western mediterranean: lidar, sun photometer observations, and regional dust modeling, J. Geophys. Res., 111, 1–16, 2006.

Pineda, N., Jorba, O., Jorge, J., and Baldasano, J. M.: Using NOAA AVHRR and SPOT VGT data to estimate surface parameters: application to a mesoscale meteorological model, Int. J. Remote Sens., 25, 129–143, 2004.

Queen, A. and Zhang, Y.: Examining the sensitivity of MM5-CMAQ predictions to explicit microphysics schemes and horizontal grid resolutions, Part III – The impact of horizontal grid resolution, Atmos. Environ., 42, 3869–3881, 2008.

San José, R., Pérez, J. L., Morant, J. L., and González Barras, R. M.: The use of Modern third-generation air quality models (MM5-EMIMO-CMAQ) for real-time operational air quality impact assessment of industrial plants, Water Air Soil Poll., 9, 27–37, 2009.

Skamarock, W. C. and Klemp, J. B.: A time-split nonhydrostatic atmospheric model for weather research and forecasting applications, J. Comput. Phys., 227, 3465–3485, doi:10.1016/j.jcp.2007.01.037, 2008.

Szopa, S., Foret, G., Menut, L., and Cozic, A.: Impact of large scale circulation on European summer surface ozone and consequences for modelling forecast, Atmos. Environ., 43, 1189–1195, 2009.

Tesche, T. W., Morris, R., Tonnesen, G., McNally, D., Boylan, J., and Brewer, P.: CMAQ/CAMx annual 2002 performance evaluation over the eastern US, Atmos. Environ., 40, 4906–4919, 2006.

Timmermans, R. M. A., Denier van der Gon, H. A. C., Kuenen, J. J. P., Segers, A. J., Honoré, C., Perrussel, O., Builtjes, P. J. H., and Schaap, M.: Quantification of the urban air pollution increment and its dependency on the use of down-scaled and bottom-up city emission inventories, Urban Climate, 6, 44–62, 2013.

Toll, I. and Baldasano, J. M.: Modeling of photochemical air pollution in the Barcelona area with highly disaggregated anthropogenic and biogenic emissions, Atmos. Environ., 34, 3060–3084, 2000.

Valari, M. and Menut, L.: Does an increase in air quality models' resolution bring surface ozone concentrations closer to reality?, J. Atmos. Ocean. Technol., 25, 1955–1968, 2008.

Valverde, V. V., Pay, M. T., and Baldasano, J. M.: Climatic synoptic classification over the Iberian Peninsula oriented to air quality dynamic characterization, Int. J. Climatol., submitted, 2014.

Vivanco, M., Correa, M., Azula, O., Palomino, I., and Martín, F.: Influence of model resolution on ozone predictions over Madrid area (Spain), in: Computational Science and its Applications – ICCSA 2008, Springer, Berlin, Heidelberg, 165–178, 2008.

WHO: Review of evidence on health aspects of air pollution – REVIHAAP Project Technical report, World Health Organization, Regional Office for Europe, Copenhagen, Denmark, 2013.

Yarwood, G., Roa, S., Yocke, M., and Whitten, G.: Updates to the carbon bond chemical mechanism: CB05, Final report to the US EPA, RT-0400675, 2005.

Zhang, K., Knipping, E., Wexler, A., Bhave, P., and Tonnensen, G.: Size distribution of sea-salt emissions as a function of relative humidity, Atmos. Environ., 39, 3373–3379, 2005.

Zhang, Y., Bocquet, M., Mallet, V., Seigneur, C., and Baklanov, A.: Real-time air quality forecasting, Part I: History, techniques, and current status, Atmos. Environ., 60, 632–655, 2012.

Title Page

Abstract | Introduction

Conclusions | References

Tables | Figures

◄ | ►►|

◄ | ►

Back | Close

Full Screen / Esc

Printer-friendly Version

Interactive Discussion

Table 1. CALIOPE-AQFS computational requirements in terms of Central Processors Units (CPU) and computational time (in min), for simulating 48 h air quality forecasts as a function of the domain: IP-4 km (D2), AND-1 km (D3), BCN-1 km (D5) and MAD-1 km (D4) described in Fig. 1.

	IP-4 km (399 × 399 cells)	AND-1 km (366 × 358 cells)	BCN-1 km (146 × 146cells)	MAD-1 km (146 × 158 cells)
Meteorological Modeling	128 CPU/15 min	256 CPU/80 min	128 CPU/20 min	128 CPU/20 min
Emission Modeling	1 CPU/4 min	1 CPU/4 min	1 CPU/1 min	1 CPU/1 min
Air Quality modeling	256 CPU/210 min	256 CPU/220 min	128 CPU/150 min	128 CPU/110 min

Table 2. Discrete and categorical statistics for NO_2, O_3, O_3-8 h, and PM_{10} for April 2013 as a function of horizontal resolution (4 km and 1 km). n indicates the number of pairs of data used in the discrete evaluation on an hourly basis. OM and MM depict the measured and modeled mean concentrations, respectively. T is the threshold applied in the categorical evaluation. Max 1 h and mean 24 h concentrations are calculated considering $\geq 75\%$ of the hours in a day, as establish in the Directive 2008/50/EC.

	NO_2		O_3		O_3-8 h		PM_{10}	
n (stations)	90 761 (135)		76 471 (114)		3248 (114)		66 642 (100)	
OM ($\mu g\,m^{-3}$)	22.0		68.4		88.6		20.6	
EU LV/TV ($\mu g\,m^{-3}$) (temp basis)	200 (Max 1 h)		180 (Max 1 h)		120 (Max 8 h)		50 (Mean 24 h)	
EU LV/TV exceedances	0		25		0		31	
T^* ($\mu g\,m^{-3}$) (temp. basis)	71 (Max 1 h)		108 (Max 1 h)		101 (Max 8 h)		27 (Mean 24 h)	
Discrete evaluation								
	4 km	1 km	4 km	1 km	4 km	1 km	4 km	1 km
MM ($\mu g\,m^{-3}$)	17.4	19.3	58.0	57.3	72.4	71.5	13.9	14.0
r	0.54	0.54	0.61	0.61	0.54	0.51	0.45	0.44
MB ($\mu g\,m^{-3}$)	−4.5	−2.6	−10.5	−11.3	−16.3	−17.2	−6.7	−6.6
MAE ($\mu g\,m^{-3}$)	12.9	13.2	19.7	19.8	18.4	19.2	12.6	12.7
RMSE ($\mu g\,m^{-3}$)	19.8	20.4	24.6	24.7	21.8	22.8	17.2	17.4
MNBE (%)	−20.4	−11.8	−15.3	−16.5	−18.4	−19.4	−32.5	−32.0
MNGE (%)	58.5	59.9	28.8	28.9	20.8	21.7	61.1	61.6
MFB (%)	−28.5	−23	−13.1	−15.1	−19.3	−20.5	−63.3	−64.1
MFE (%)	69.2	68.7	37.1	37.4	22.5	23.5	85.7	87.1
Categorical evaluation (Threshold = T^*)								
	4 km	1 km	4 km	1 km	4 km	1 km	4 km	1 km
a (false alarm)	306	384	41	19	17	6	131	133
b (hits)	466	537	112	96	6	4	331	334
c (correct negative)	2517	2439	1846	1868	2826	2837	1978	1976
d (misses)	487	416	1194	1210	399	401	334	331
B (%, 100)	37	40	8	7	1	1	42	42
POD (%, 100)	49	56	9	7	1	1	50	50
CSI (%, 100)	81	97	12	9	6	2	69	70
FAR (%, 0)	40	42	27	17	74	60	28	28
A (%, 100)	79	79	61	62	87	87	83	83

T^* is defined as the 75p of the observed concentrations estimated on the temporal basis established in the EU Directive 2008/50/EC.
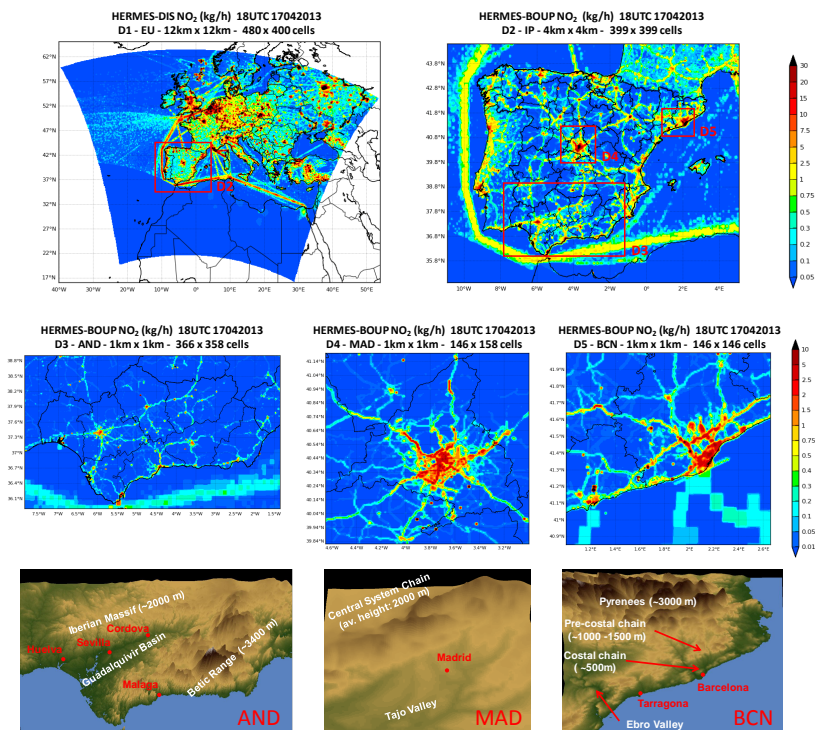
Fig. 1. CALIOPE-AQFS nesting strategy and topography for each study domains: Andalucia (AND), Madrid (MAD), and Barcelona (BCN). Colour chart at D-domains shows NO_2 emission rate (kg h^{-1}) for 17 April 2013 at 18:00 UTC. HERMES-DIS model generates emission at 12 km × 12 km over Europe (the mother domain, D1) by means disaggregation from EMEP database. HERMES-BOUP model estimates emissions at 1 km × 1 km following a bottom-up approach.
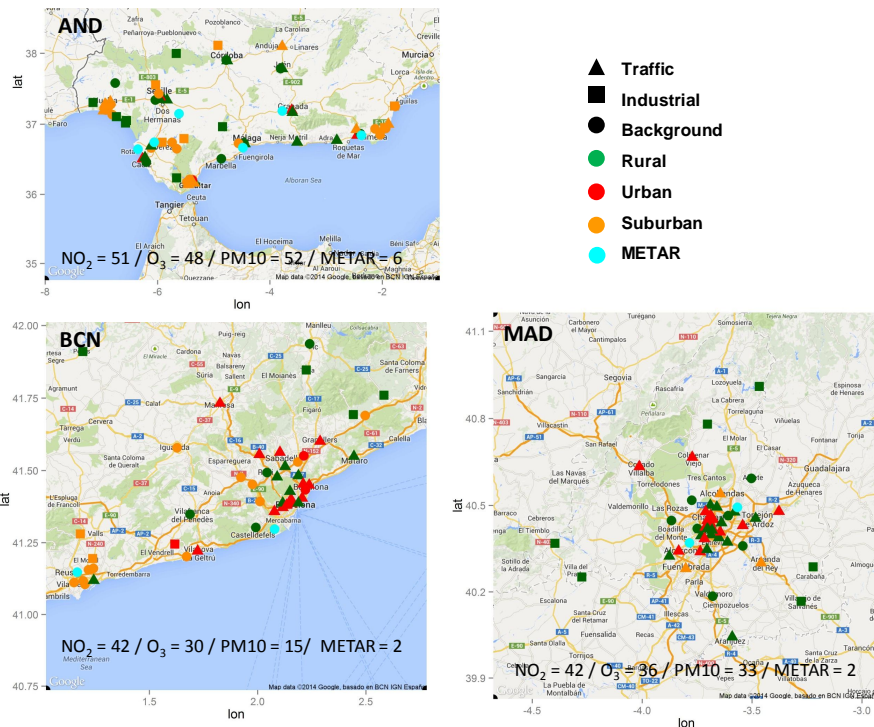
Fig. 2. Air quality stations for NO_2, O_3 and PM_{10} at the three domains at hands (AND, BCN and MAD) in April 2013. Different types of stations are showed by symbols and color codes. The various symbols represent the major emission type affecting each station (Traffic: triangle; Industrial: square; and Background: circle), while the colors reflect the environment of each station (Urban: red; Suburban: green; and Rural: orange). Cyan dots represent METAR stations used in Sect. S1.
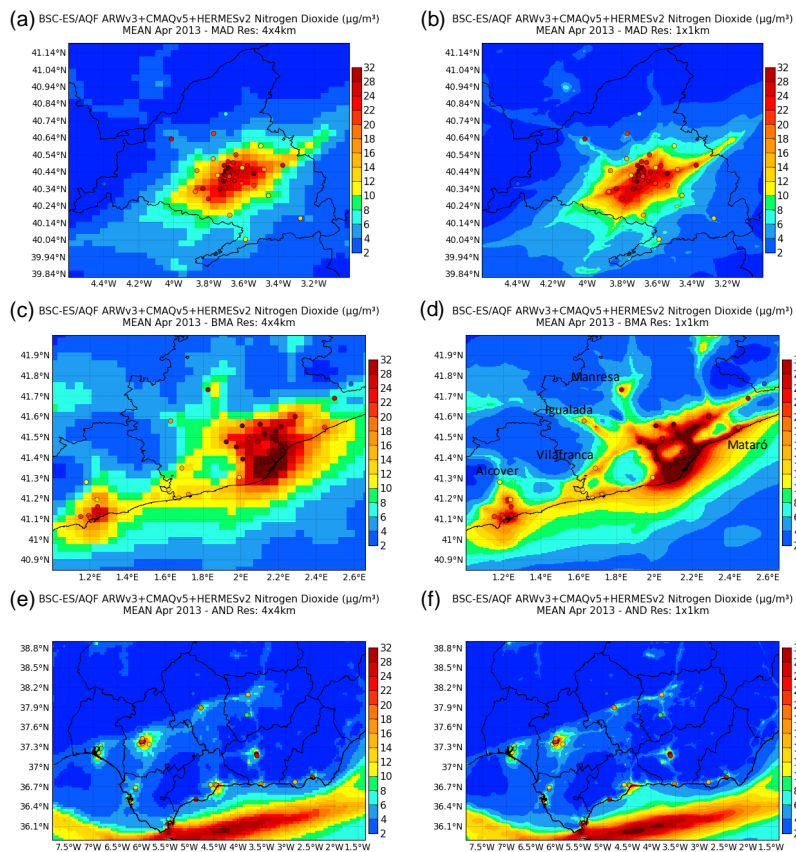
Fig. 3. CALIOPE-AQFS mean NO$_2$ concentration (μg m^{-3}) in April 2013 over **(a, b)** MAD, **(c, d)** BCN, and **(e, f)** AND as a function of horizontal resolution: 4 km (left column) and 1 km (right column). Dots indicate mean concentration at air quality stations.

Fig. 4. CALIOPE-AQFS mean O$_3$ concentration ($\mu g\, m^{-3}$) in April 2013 over **(a, b)** MAD, **(c, d)** BCN, and **(e, f)** AND as a function of horizontal resolution: 4 km (left column) and 1 km (right column). Dots indicate mean concentration at air quality stations.
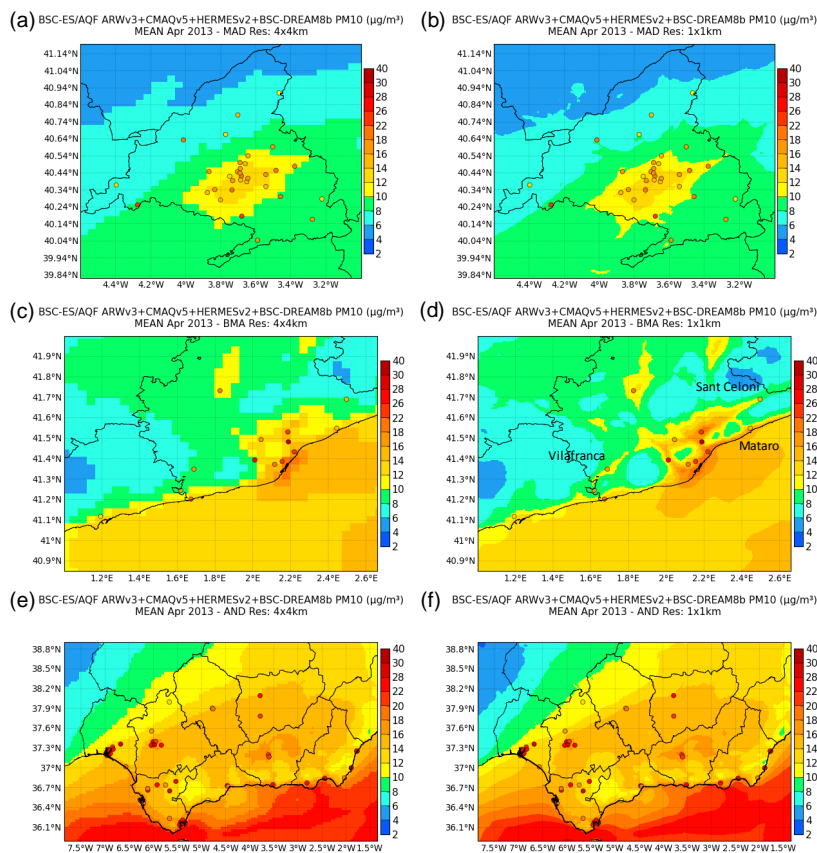
Fig. 5. CALIOPE-AQFS mean PM$_{10}$ concentration (μg m^{-3}) in April 2013 over **(a, b)** MAD, **(c, d)** BCN, and **(e, f)** AND as a function of horizontal resolution: 4 km (left column) and 1 km (right column). Dots indicate mean concentrations at air quality stations.

Title Page

Abstract | Introduction

Conclusions | References

Tables | Figures

|◄ | ►|

◄ | ►

Back | Close

Full Screen / Esc

Printer-friendly Version

Interactive Discussion
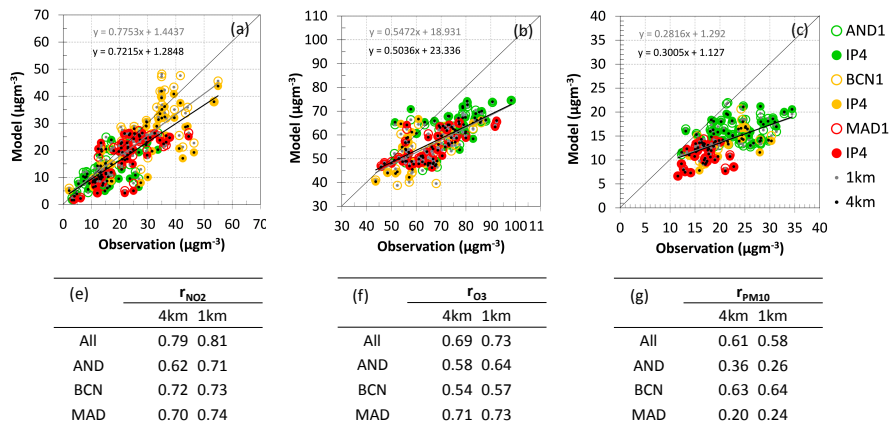
Fig. 6. Monthly mean scatter plots for CALIOPE-AQFS (y-axis) and observed (x-axis) concentrations for the three study domains (AND in green, BCN in yellow; and MAD in red) as a function of horizontal resolution for **(a)** NO$_2$, **(b)** O$_3$ and **(c)** PM$_{10}$. Equations show the linear adjust between models and observations at 1 km (light grey) and 4 km (dark grey). Spatial correlation coefficients as a function of resolution and domain are shown for **(e)** NO$_2$, **(f)** O$_3$, and **(g)** PM$_{10}$.

Title Page

Abstract | Introduction

Conclusions | References

Tables | Figures

|◄ | ►|

◄ | ►

Back | Close

Full Screen / Esc

Printer-friendly Version

Interactive Discussion
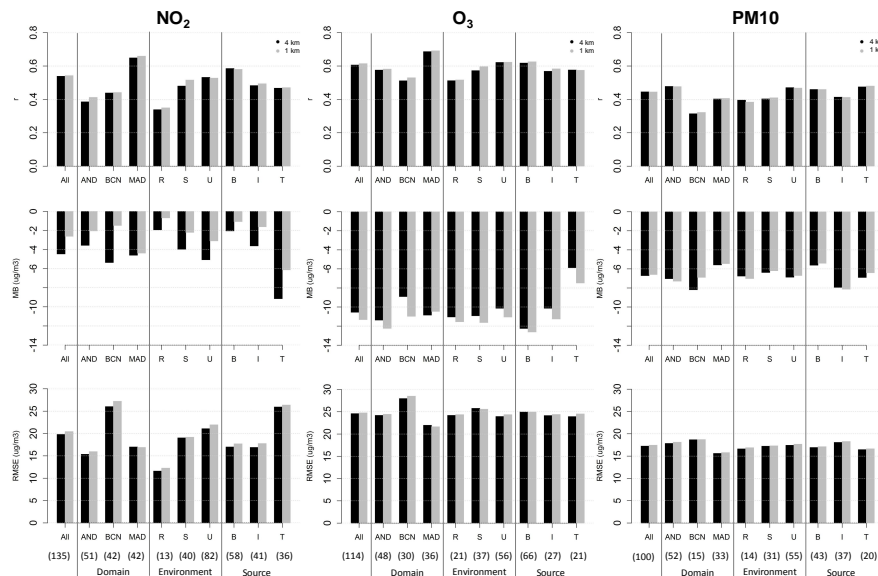
Fig. 7. Statistics (r, MB, and RMSE in rows) for each pollutant (NO_2, O_3, and PM_{10} in columns) on an hourly basis as a function of horizontal resolution, 4 km (black) and 1 km (grey). Four categories are considered: all stations (all), domain (AND, BCN and MAD), station environment (R, S, and U), and main sources (B, I, and T).
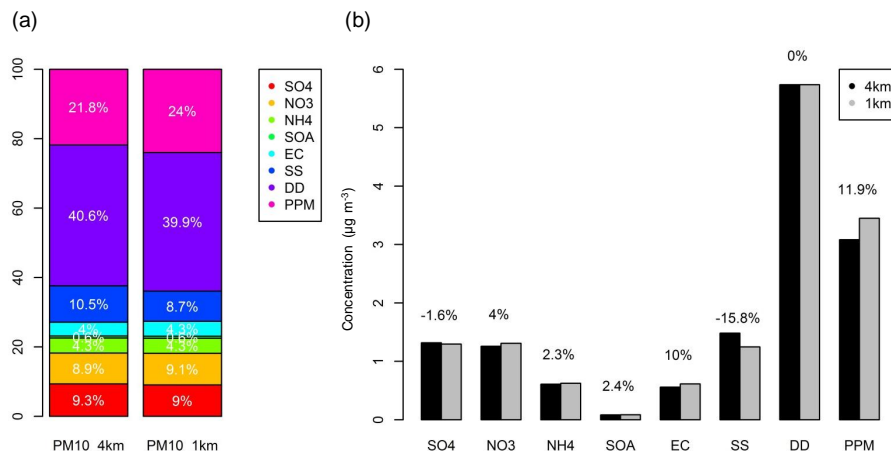
Fig. 8. Resolution effect on PM$_{10}$ components in April 2013. **(a)** Percentage of PM$_{10}$ components: sulfate (SO4), nitrate (NO3), ammonium (NH4), secondary organic aerosol (SOA), elemental carbon (EC), sea salt (SS), desert dust (DD), and primary particulate matter (PPM). **(b)** PM$_{10}$ component concentrations at 1 km simulation (black) and 4 km simulation (grey). Numbers over bars indicate the % of increase when increasing resolution.

Title Page

Abstract | Introduction

Conclusions | References

Tables | Figures

|◄ | ►|

◄ | ►

Back | Close

Full Screen / Esc

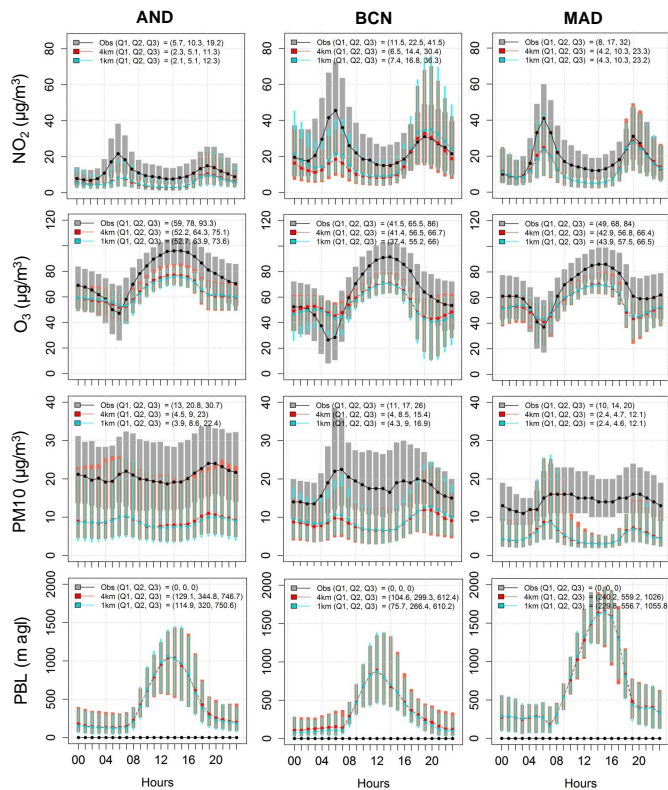Printer-friendly Version

Interactive Discussion

Fig. 9. Daily cycles for NO_2, O_3 and PM_{10} for each study domain at available stations as a function of resolution. No observations of PBL are available. Q1, Q2 and Q3 indicate quartiles for the daily cycle. Bars show Q1 and Q3 at each hour.
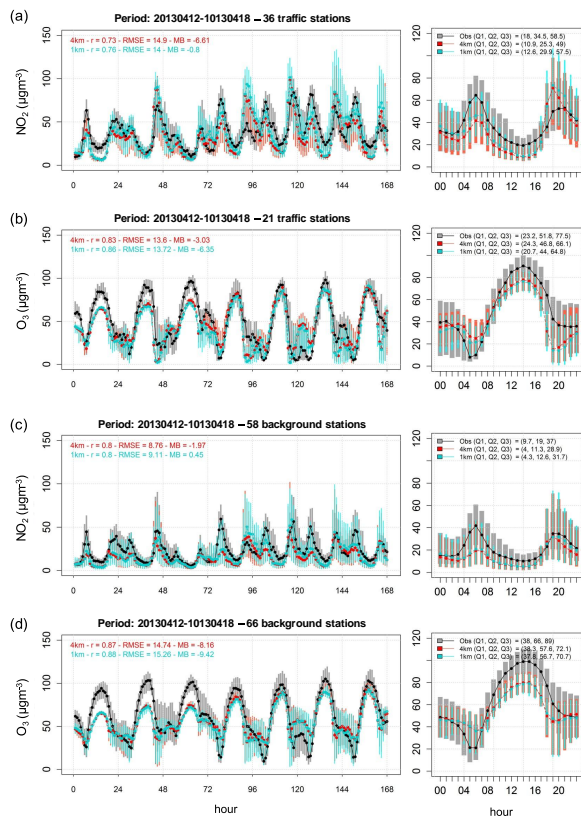
Fig. 10. Temporal series and daily cycles for NO_2 and O_3 at background (**a** and **b**, respectively) and traffic stations (**c** and **d**, respectively) for the episode 12–18 April 2013. Q1, Q2 and Q3 indicate quartiles for the daily cycle. Bars show Q1 and Q3 at each hour.